DESIGN OF DIELECTRIC RESONATOR ANTENNAS USING SURROGATE-BASED OPTIMIZATION AND ELECTROMAGNETIC MODELS

Slawomir Koziel, Stanislav Ogurtsov and Leifur Leifsson
Engineering Optimization & Modeling Center, School of Science and Engineering
Reykjavik University, 101 Reykjavik, Iceland

Keywords: Dielectric resonator antennas, Microwave design, Design optimization, Surrogate models.

Abstract: Design of dielectric resonator antennas (DRAs) is a challenging task because their analytical models are only appropriate for estimation, i.e., to calculate the resonance frequency and radiation quality factor of an isolated dielectric resonator or for obtaining an initial design. In practice, the geometry parameters that ensure satisfaction of performance requirements are often obtained by repetitive electromagnetic (EM) simulations guided by engineering experience. This is a tedious process, and it does not guarantee optimal results. On the other hand, employing the EM solver directly in the optimization loop is typically impractical because high-fidelity EM simulations are computationally expensive. Here, we describe several techniques that allow designing DRAs in a computationally efficient way. All presented methods exploit coarse-discretization EM models of the DRA. These models, after correction, serve as prediction tools that guide the optimization process. As the low-fidelity models are computationally much cheaper than the original, high-fidelity ones, the cost of the design process is greatly reduced. The approaches presented here include adaptively adjusted design specifications, shape-preserving response prediction, and space mapping with kriging-based coarse models. Antenna design examples are provided.

1 INTRODUCTION

Dielectric resonator antennas (DRAs) possess a number of features which make them attractive for engineers and designers (Kishk et al., 2007; Petosa, 2007): a wide frequency range of operation (1-to-44 GHz); compact size compared to their counterparts like microstrip antennas; different radiation patterns for various requirements; variety of feeding schemes (such as probes, slots, microstrip, coplanar waveguide, dielectric image guide); wider impendence bandwidth compared with microstrip antennas and attributed to the DRA radiation mechanism; wide temperature range of operation; high power handling capability.

DRA design involves adjustment of geometry in order to satisfy application specific requirements. In most cases, available analytical models (Kishk et al., 2007; Petosa, 2007) can only be used to estimate the resonant frequency and radiation quality factor of the isolated dielectric resonator. For accurate DRA responses full-wave electromagnetic (EM) simulation is necessary to account for the environment (e.g., installation platform, housing, feeding circuit). Therefore, EM-simulation-based optimization seems to be the only reliable option for DRA design. However, the bottleneck is high computational cost: high-fidelity simulation may take up to a few hours even for a single set of design variables. As a result, approaches based on the direct use of the EM solver in an optimization loop are impractical. In practice, search for optimal DRA dimensions is typically realized as a simulation-based parametric study, e.g., (De Young et al., 2006; Guo et al., 2005; Ong et al., 2002), or measurement of multiple prototypes, e.g., (Petosa, 2007); unfortunately, both approaches are tedious and do not guarantee optimality of the final design.

Efficient simulation-driven design can be realized using surrogate-based optimization (SBO) (Queipo et al., 2005; Forrester et al., 2009). In SBO the computational burden is shifted to a surrogate model, a computationally cheap representation of the optimized structure. SBO approaches, shown to be successful in microwave area, include space mapping (SM) (Bandler et al., 2004; Amari et al., 2006; Koziel et al., 2006; Koziel et al., 2008), tuning

Koziel S., Ogurtsov S. and Leifsson L..
DESIGN OF DIELECTRIC RESONATOR ANTENNAS USING SURROGATE-BASED OPTIMIZATION AND ELECTROMAGNETIC MODELS.
DOI: 10.5220/0003571404390448
In *Proceedings of 1st International Conference on Simulation and Modeling Methodologies, Technologies and Applications* (SDDOM-2011), pages 439-448
ISBN: 978-989-8425-78-2
Copyright © 2011 SCITEPRESS (Science and Technology Publications, Lda.)

(Rautio, 2007) and tuning SM (Koziel et al., 2009). Unfortunately, applicability of these techniques for antennas is limited. SM normally relies on a fast coarse model, typically, circuit equivalent (Bandler et al., 2004). Regrettably, reliable circuit equivalents are not available for DRAs due to the underlying EM phenomena. On the other hand, simulation-based tuning is not directly applicable for radiating structures.

Recently, there has been tendency to use meta-heuristic approaches (Yang, 2010) for antenna design, e.g., genetic algorithms (Haupt, 2008), particle swarm optimizers (Lizzi et al., 2006), and ant colony optimization (Rocca et al., 2008). While these techniques alleviate some optimization problems, e.g., handling multiple local optima, they normally require massive amounts of objective function calls. Therefore, meta-heuristic approaches are not well suited for the DRA design purposes.

Here, we discuss three simulation-driven optimization methodologies that are suitable for DRA design. All of them exploit coarse-discretization EM simulations as the low-fidelity models. Such models are not as accurate as the original, high-fidelity simulations, but they are computationally much cheaper. After suitable correction, these low-fidelity models can be used in place of high-fidelity ones in the optimization process. We focus on three design optimization approaches that are straightforward to implement, and yet computationally efficient.

The first technique, shape-preserving response prediction (SPRP) (Koziel, 2010b), creates a reliable surrogate of the DRA by aligning the simulation results of its low-fidelity model with that of its high-fidelity model. The surrogate serves as a predictor estimating the optimal geometry. The second technique does not apply any corrections to the coarse-discretization models directly. Instead, the discrepancy between the low- and high-fidelity models is accounted for by modification of design specifications (Koziel, 2010a). The last methodology exploits SM as the optimization engine with the underlying coarse model created by kriging interpolation of the coarse-discretization simulation data (Koziel, 2009b).

Examples are provided for the described techniques. In all cases, the final design is obtained at a low computational cost corresponding to a few high-fidelity EM simulations of the antenna under consideration.

2 DRA DESIGN USING SURROGATE MODELS

2.1 Design Problem Formulation

For the sake of this work, the DRA design is formulated as a nonlinear minimization problem of the form

$$\boldsymbol{x}_f^* = \arg\min_{\boldsymbol{x}} U\left(\boldsymbol{R}_f(\boldsymbol{x})\right) \quad (1)$$

where $\boldsymbol{R}_f(\boldsymbol{x}) \in R^m$ is the response vector of a high-fidelity (fine) model of the antenna of interest; U is a given objective function (e.g., typically minimax (Bandler et al., 2004)), whereas $\boldsymbol{x} \in R^n$ is a vector of design variables, typically, the geometry parameters. The most common objective in the antenna design is to minimize so-called reflection coefficient $|S_{11}|$ over certain frequency band of interest. Other objectives may concern the antenna gain or the shape of the radiation pattern. It is assumed that the computational cost of evaluating the high-fidelity model is high so that solving (1) directly is impractical.

2.2 Surrogate-based Optimization. Low-fidelity Models

The SBO techniques exploiting physics-based low-fidelity models can be particularly efficient (Bandler et at., 2004). As mentioned before, space mapping (Koziel et al., 2008) and simulation-based tuning (Rautio, 2007) are both highly efficient approaches, however, their applicability is limited to devices where fast circuit equivalents are readily available, e.g., in the case of microstrip filters (Bandler et al., 2004; Amari et al., 2006).

Here, we exploit the models obtained through coarse-discretization of the original structure (referred to as $\boldsymbol{R}_c$). The major advantage is that such models are available for any DRA. Moreover, coarse-discretization models can be implemented with the same EM solver, as that of the corresponding high-fidelity models, by applying relaxed mesh requirements. The use of the same solver simplifies implementation of the optimization algorithm. On the other hand, coarse-discretization EM models are still relatively expensive when compared to circuit equivalents. For that reason, we look for optimization techniques that are capable to reduce not only the number of evaluations of the high-fidelity model, but also the number of coarse-discretization simulations so that the computational overhead related to low-fidelity model evaluations does not affect the total design cost significantly. In

particular, coarse-discretization EM models are normally too expensive to serve as immediate coarse models for efficient SM implementation. This would be particularly problematic for the parameter extraction step of SM which requires a substantial number of model evaluations (Koziel et al., 2006).

In the remaining part of this section we discuss a few optimization approaches utilizing coarse-discretization EM models that are suitable for DRA design. These methods are simple to implement and computationally efficient. Application examples are provided in Section 3.

2.3 Shape-Preserving Response Prediction

The shape-preserving response prediction (SPRP) method (Koziel, 2010b) exploits the iterative process

$$\boldsymbol{x}^{(i+1)} = \arg\min_{\boldsymbol{x}} U\left(\boldsymbol{R}_s^{(i)}(\boldsymbol{x})\right) \quad (2)$$

where $\boldsymbol{R}_s^{(i)}$ is the surrogate model at iteration i, whereas $\boldsymbol{x}^{(i+1)}$ is the approximate solution to (1) obtained by optimizing $\boldsymbol{R}_s^{(i)}$. In SPRP, the surrogate is constructed under the assumption that the change of the high-fidelity model response due to the adjustment of the design variables can be predicted using the actual changes of the low-fidelity model response. This property is ensured by the low-fidelity model being the coarse-mesh simulation of the same DRA structure that represents the high-fidelity one.

The change of the low-fidelity model response can be described by the translation vectors corresponding to so-called characteristic points of the model's response. These translation vectors are subsequently used to predict the change of the high-fidelity model response with the actual response of $\boldsymbol{R}_f$ at the current iteration point, $\boldsymbol{R}_f(\boldsymbol{x}^{(i)})$, treated as a reference.

Figure 1(a) shows the example low-fidelity model response, $|S_{11}|$ versus frequency, at the design $\boldsymbol{x}^{(i)}$, as well as the coarse model response at some other design $\boldsymbol{x}$. The responses come from the dielectric resonator antenna considered in Section 3.1. Circles denote characteristic points of $\boldsymbol{R}_c(\boldsymbol{x}^{(i)})$, selected here to represent $|S_{11}| = -10$ dB, $|S_{11}| = -15$ dB, and the local $|S_{11}|$ minimum. Squares denote corresponding characteristic points for $\boldsymbol{R}_c(\boldsymbol{x})$, while line segments represent the translation vectors ("shift") of the characteristic points of $\boldsymbol{R}_c$ when changing the design variables from $\boldsymbol{x}^{(i)}$ to $\boldsymbol{x}$.

The high-fidelity model response at $\boldsymbol{x}$ can be predicted using the same translation vectors applied to the corresponding characteristic points of the high-fidelity model response at $\boldsymbol{x}^{(i)}$, $\boldsymbol{R}_f(\boldsymbol{x}^{(i)})$. This is illustrated in Fig. 1(b). Figure 1(c) shows the predicted versus actual high-fidelity model response at $\boldsymbol{x}$. Rigorous formulation of SPRP can be found in (Koziel, 2010b). It is omitted here for the sake of brevity.

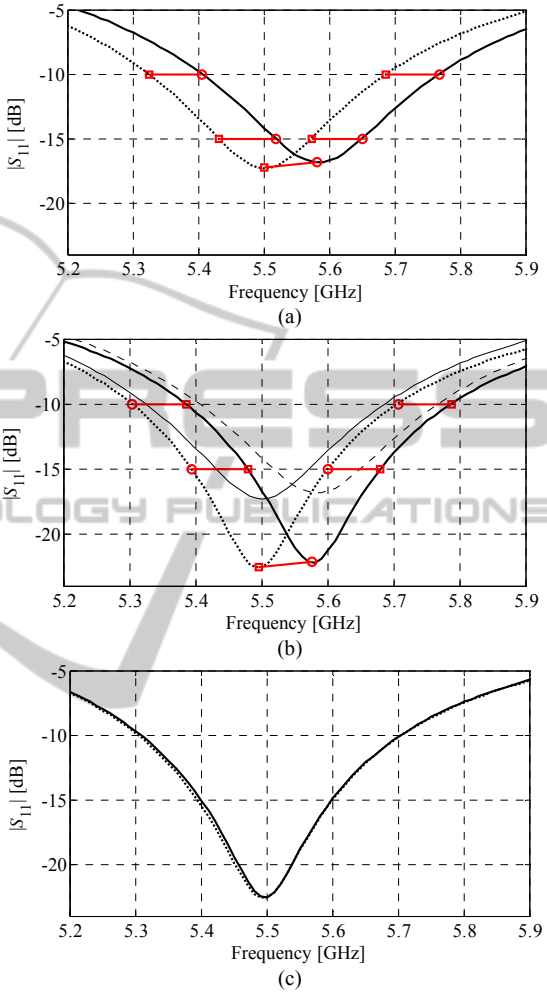

Figure 1: SPRP concept: (a) Low-fidelity model response at the design $\boldsymbol{x}^{(i)}$, $\boldsymbol{R}_c(\boldsymbol{x}^{(i)})$ (—), the low-fidelity model response at $\boldsymbol{x}$, $\boldsymbol{R}_c(\boldsymbol{x})$ (····), characteristic points of $\boldsymbol{R}_c(\boldsymbol{x}^{(i)})$ (o) and $\boldsymbol{R}_c(\boldsymbol{x})$ (□), and the translation vectors (▬); (b) High-fidelity model response at $\boldsymbol{x}^{(i)}$, $\boldsymbol{R}_f(\boldsymbol{x}^{(i)})$ (—) and the predicted high-fidelity model response at $\boldsymbol{x}$ (····) obtained using SPRP based on characteristic points of (a); characteristic points of $\boldsymbol{R}_f(\boldsymbol{x}^{(i)})$ (o) and the translation vectors (▬) were used to find the characteristic points (□) of the predicted high-fidelity model response; (c) low-fidelity model responses $\boldsymbol{R}_c(\boldsymbol{x}^{(i)})$ and $\boldsymbol{R}_c(\boldsymbol{x})$ are plotted using thin solid and dotted line, respectively.

2.4 Adaptively Adjusted Design Specifications

It is not necessary to remove the discrepancies

between the low- and high-fidelity models by correcting the low-fidelity model. Another way is to "absorb" the model misalignment by proper adjustment of the design specifications. In microwave engineering, most of the design tasks can be formulated as minimax problems with upper and lower specifications and it is easy to implement modifications by, for example, shifting the specification levels, corresponding frequency bands (Koziel, 2010a).

The optimization procedure exploiting this idea consists of the following two simple steps:

1. Modify the original design specifications to account for the discrepancy between the low- and high-fidelity models.
2. Obtain a new design by optimizing the low-fidelity model with respect to the modified specifications.

In Step 1, the design specifications are modified so that the level of satisfying/violating the modified specifications by the low-fidelity model response corresponds to the satisfaction/violation levels of the original specifications by the high-fidelity model (Koziel, 2010a). The low-fidelity model is then optimized in Step 2 with respect to the modified specifications and the new design obtained this way is treated as an approximated solution to the original design problem, i.e., optimization of the high-fidelity model with respect to the original specifications. Because the low-fidelity model is physics-based, the adjustment of the design variables has similar effect on the response for both the low- and high-fidelity models. As a result, the low-fidelity model design obtained in Step 2 (i.e., optimal with respect to the modified specifications) will be (almost) optimal for the high-fidelity model with respect to the original specifications.

Steps 1 and 2 can be repeated if necessary. Typically, a substantial improvement is observed after the first iteration. Additional iterations may bring further enhancement as the discrepancy between the high- and low-fidelity models may change from one design to another.

Figure 2 illustrates an iteration of our technique used for design of a CBCPW-to-SIW transition (Deslandes and Wu, 2005). One can observe that the absolute matching between the low- and high-fidelity models is not as important as the shape similarity.

2.5 Optimization using Space Mapping and Kriging-based Coarse Models

Similarly as SPRP, space mapping (SM) (Bandler et al., 2004) solves the original design problem (1)

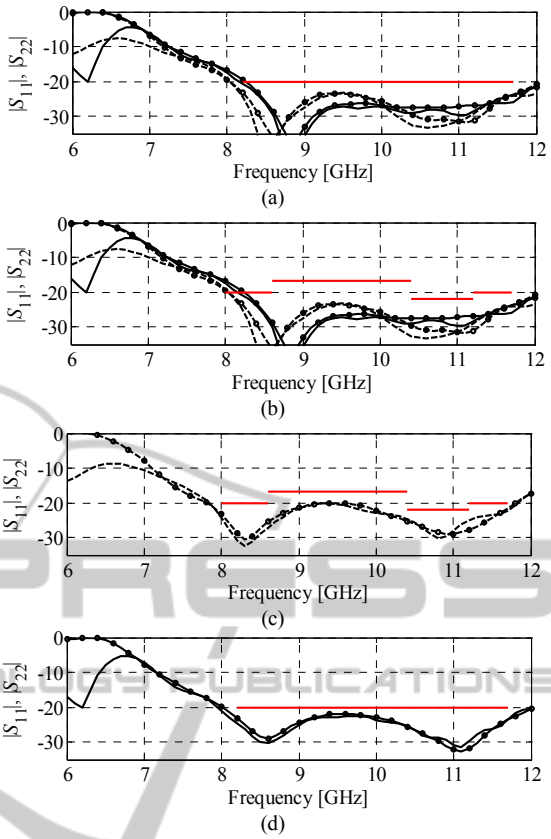

Figure 2: Adaptively adjusted design specification technique applied to optimize CBCPW-to-SIW transitions. High- and low-fidelity model response denoted as solid and dashed lines, respectively. $|S_{22}|$ distinguished from $|S_{11}|$ using circles. Design specifications denoted by thick horizontal lines. (a) High- and low-fidelity model responses at the beginning of the iteration as well as original design specifications; (b) High- and low-fidelity model responses and modified design specifications that reflect the differences between the responses; (c) Low-fidelity model optimized to meet the modified specifications; (d) high-fidelity model at the low-fidelity model optimum shown versus original specifications. Thick horizontal lines indicate the design specifications.

using an iterative procedure (2) (cf. Section 2.3). SM surrogate is also constructed from the low-fidelity model $\boldsymbol{R}_c$ by applying suitable transformation of the model parameter space and/or response. A variety of SM surrogate models are available (Koziel et al., 2006). A specific model used in this work is defined as $\boldsymbol{R}_s^{(i)}(\boldsymbol{x}) = \boldsymbol{R}_c(\boldsymbol{x} + \boldsymbol{c}^{(i)}) + \boldsymbol{d}^{(i)}$. The vector $\boldsymbol{c}^{(i)}$ is obtained in the parameter extraction process $\boldsymbol{c}^{(i)} = \text{argmin}\{\boldsymbol{c} : \|\boldsymbol{R}_f(\boldsymbol{x}^{(i)}) - \boldsymbol{R}_c(\boldsymbol{x}^{(i)} + \boldsymbol{c})\|\}$ which aims at reducing misalignment between the high- and SM-mapped low-fidelity model responses at $\boldsymbol{x}^{(i)}$. The vector $\boldsymbol{d}^{(i)}$ is calculated as $\boldsymbol{d}^{(i)} = \boldsymbol{R}_f(\boldsymbol{x}) - \boldsymbol{R}_c(\boldsymbol{x} + \boldsymbol{c}^{(i)})$. The parameter shift $\boldsymbol{x} + \boldsymbol{c}^{(i)}$ is referred to as input

SM, while the response correction through the vector $\boldsymbol{d}^{(i)}$ is called output SM (Bandler et al., 2004).

Space mapping is a flexible and general surrogate-based optimization methodology (Bandler et al., 2004), however, its application to DRA design may not be straightforward because SM requires a physically-based and yet computationally cheap low-fidelity model (preferably, an equivalent circuit). The use of coarse-discretization EM models as the low-fidelity model may be problematic because the SM algorithm typically requires a large number of low-fidelity model evaluations, particularly in the parameter extraction step (Koziel et al., 2008). As EM simulations, even low-fidelity ones, are relatively expensive (typically, only 10 to 50 times faster than the high-fidelity models), the efficiency of the SM algorithm could be compromised because of numerous evaluations of the coarse-discretization model.

The workaround is to build a (local) function approximation model using coarse-discretization model data, and treat it as a low-fidelity model for the space mapping algorithm (Koziel, 2009b). This approach has several advantages: (i) $\boldsymbol{R}_c$ model is computationally cheap, smooth, and therefore, easy to optimize, (ii) there is no need for circuit-equivalent model, and, consequently, no extra simulation software needs to be involved; the space mapping algorithm implementation is simpler and exploits a single EM solver, (iii) it is possible to apply SM for DRA design problems where finding reliable and fast low-fidelity models is difficult or impossible. Here, we use kriging (Queipo et al., 2005) as a function approximation technique.

The design procedure is the following:

1. Starting from $\boldsymbol{x}^{init}$, find an approximate optimal design $\boldsymbol{x}^{(0)}$ of the coarse-discretization model $\boldsymbol{R}_{cd}$. In this work, we use a pattern search algorithm (Kolda et al., 2003).
2. Sample $\boldsymbol{R}_{cd}$ in the vicinity of $\boldsymbol{x}^{(0)}$ and construct a response surface approximation model $\boldsymbol{R}_c$.
3. Find a high-fidelity model optimum by applying the algorithm (2) with the surrogate model created using $\boldsymbol{R}_c$ as an underlying low-fidelity model.

The surrogate constructed by means of coarse-discretization model data and the SM alignment is a good prediction tool. It allows us to locate the high-fidelity model optimum in a few iterations (each iteration amounts to just one evaluation of the high-fidelity model) so that the entire design process is computationally inexpensive.

3 DESIGN EXAMPLES

In this section, we present several DRA design examples exploiting the methodologies described in Section 2.

3.1 DRA Design using SPRP

Consider a rectangular DRA at a metal ground (Petosa, 2007) shown in Fig. 3. The DRA is fed with a 50 ohm microstrip through a ground plane slot. The design variables are $\boldsymbol{x} = [a_x\ a_y\ a_z\ a_{y0}\ u_s\ w_s\ y_s]^T$, where a_x, a_y, and a_z are dimensions of the dielectric resonator (DR), a_{y0} stands for the shift of the DR center in Y-direction relative to the slot center, u_s is the slot width, w_s is the slot length, and y_s is the length of the microstrip stub. Relative permittivity and loss tangent of the DR are 10 and 10^{-4}, respectively. Substrate thickness is 0.5 mm. The width of the microstrip signal trace is 1.17 mm. Metallization is with 1.5 oz copper.

The design objective for reflection coefficient is $|S_{11}| \leq -10$ dB for at least 8% fractional bandwidth centered at 5.5 GHz (5.28 GHz to 5.72 GHz). The initial design is $\boldsymbol{x}^{(0)} = [8.0\ 14.0\ 8.0\ 0.0\ 1.7\ 8.4\ 8.3]^T$ mm, and it is obtained for 5.5 GHz with available design guidelines and data curves of (Petosa, 2007). However, this initial design does not meet the specifications (dot and dash lines in Fig. 4). Requirements to the DRA radiation are the following: realized gain not less than 3 dB for zero zenith angle; and, realized gain in directions down the substrate (back radiation) not greater than –15 dB, all over the frequencies where $|S_{11}|$ meets the specifications.

In the optimization process, the $|S_{11}|$ requirements are handled directly (through the objective function). The radiation requirements are treated as constraints and included into the objective function through the appropriate penalty terms.

The high-fidelity model $\boldsymbol{R}_f$ is simulated in 10 min 47 s using the CST MWS transient solver (CST, 2010) (505,250 mesh cells at the initial design). The low-fidelity model $\boldsymbol{R}_{cd}$ is also evaluated using CST MWS but with a coarser mesh (14,800 mesh cells at $\boldsymbol{x}^{(0)}$, 24 seconds).

The final design $\boldsymbol{x}^{(2)} = [8.2\ 14.2\ 8.3\ 0.0\ 1.8\ 9.4\ 7.6]^T$ mm is obtained after two iterations of the SPRP-based optimization with the total cost corresponding to about seven evaluations of the high-fidelity model (Table 1). Figure 5 shows the reflection of $\boldsymbol{R}_f$ at both the initial and the final design, as well as the response of $\boldsymbol{R}_{cd}$ at $\boldsymbol{x}^{(0)}$.

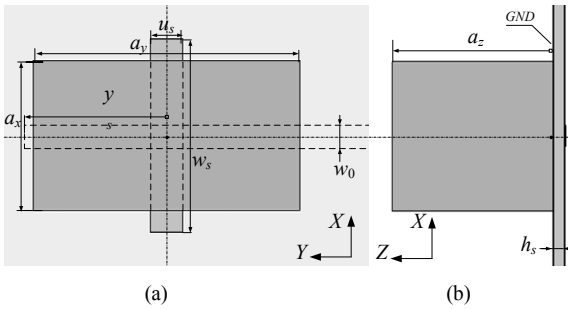

(a) (b)

Figure 3: Dielectric resonator antenna (Petosa, 2007): (a) top and (b) side views.

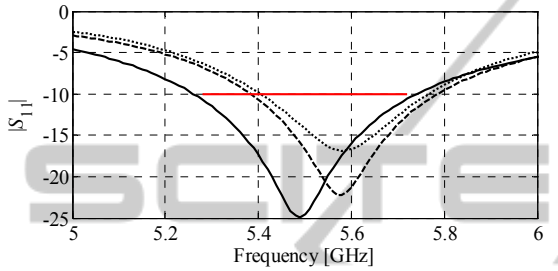

Figure 4: Dielectric resonator antenna: high- (dashed line) and low-fidelity fidelity model response (dotted line) at the initial design $\boldsymbol{x}^{(0)}$, and high-fidelity (solid line) model response at the final design.

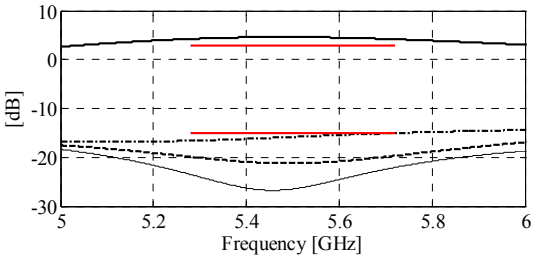

Figure 5: Realized gain of the DRA at the final design: for zenith angle of 0^0 (thick solid line); and back radiation, zenith angles of 135^0 (positive *Y*-direction, thin solid line), 180^0 (dash line), and 135^0 (negative *Y*-direction dash-dot line). Design constrains are shown with the upper horizontal line of 3 dB level and the lower line of –15 dB level.

Table 1: Rectangular DRA design: optimization cost.

Algorithm Component	Number of Model Evaluations	Evaluation Time	
		Absolute [min]	Relative to $\boldsymbol{R}_f$
Evaluation of $\boldsymbol{R}_{cd}$*	$105 \times \boldsymbol{R}_{cd}$	42	3.9
Evaluation of $\boldsymbol{R}_f$#	$3 \times \boldsymbol{R}_f$	32	3.0
Total design time	N/A	74	**6.9**

* Includes optimization of SPRP surrogate (based on $\boldsymbol{R}_{cd}$).
# Excludes evaluation of $\boldsymbol{R}_f$ at the initial design.

3.2 Stacked Ring DRA for Two Installation Scenarios using AADS

Consider an axi-symmetric DRA structure (Shum et al., 1995) shown in Fig. 6. It comprises: two $TM_{01\delta}$ ring dielectric resonators with relative permittivity, ε_{r1}, of 36, two supporting Teflon rings, Teflon filling, finite ground (t_g = 1mm). Teflon permittivity, ε_{r2}, is 2.08. The DRA is covered by a polycarbonate (ε_{r3} = 2.7) dome. Thickness of the dome shell, d, is 2 mm. Loss tangents are: 10^{-4} for the DRs, $4{\cdot}10^{-4}$ for Teflon, and 10^{-2} for the dome. Dielectrics are described using the 1st order Debye model; permittivity and loss tangent values are listed for 6 GHz. The radii of the supporting rings are equal to the radii of the DR above them. Metal parts are of copper. The inner conductor of the 50 ohm coax is extended as a probe (h_0 above the ground), and its diameter is 1.27 mm. Coax filling is Teflon.

Design variables are inner and outer radii of the DRs, heights of the DRs and the supporting rings, the probe length, dome height and radius, and radius of the DRA ground, namely, $\boldsymbol{x} = [a_1\ a_2\ b_1\ b_2\ h_1\ h_2\ g_1\ g_2\ h_0\ h_d\ r_d\ r_g]^T$. The design objective is $|S_{11}| \le -15$ dB in the band of 4-to-6 GHz for the DRA that is to be installed in two environments, see Fig. 6, one is with an infinite metal ground plane and the other is only with the DRA ground (the radius of r_g).

It should be emphasized that the above design problem is challenging for the following reasons: (i) the large number of design variables, 12, (ii) high-computational cost of simulation, (iii) design for two installation scenarios at the same time.

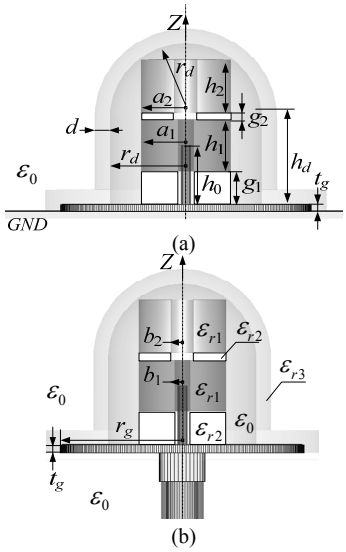

Figure 6: DRA side views: (a) DRA installed at the infinite metal ground; (b) the same DRA with its finite ground only. The feeding cable is shown on (b). Teflon filling is not shown. The dome and DRA rings are shown transparent.

The last issue not only increases the computational cost of the design process but also requires finding a trade-off between optimal designs for each environment taken separately. Solving this problem either by using parameter sweeps or by direct EM-based optimization involving high-fidelity simulations seems to be hardly feasible.

The EM models of the DRA are defined using CST MWS software and simulated using the transient solver (CST, 2010). The low-fidelity models are much faster than high-fidelity ones (in our case, about 15 times), however, they are also less accurate: the discrepancy in |S11| between low- and high-fidelity models depends on frequency and can be as large as 5 to 10 dB.

The AADS algorithm comprises the following steps:

1. Starting from $\boldsymbol{x}^{init}$, find an approximate optimal design $\boldsymbol{x}^{(0)}$ of the coarse-discretization model $\boldsymbol{R}_{cd}$. Here we use a pattern search.
2. Modify the original design specifications to take into account the difference between the responses of the low- and high-fidelity models. Obtain a new design by optimizing the low-fidelity model with respect to the modified specifications.

Design starts from $\boldsymbol{x}^{in} = [a_1\ a_2\ b_1\ b_2\ h_1\ h_2\ g_1\ g_2\ h_0\ h_d\ r_d\ r_g]^T = [6.9\ 6.9\ 1.05\ 1.05\ 6.2\ 6.2\ 2.0\ 2.0\ 6.8\ 12.0\ 10\ 16.5]^T$ which is far from meeting the design requirements (see Fig. 3(a)). At the initial design, the high-fidelity model with the finite ground has 4,369,634 mesh-cells and that with the infinite ground has 4,006,017 mesh-cells; their run times are 10,088 s and 8,697 s, respectively. The coarse-discretization model with the finite ground has 696,135 mesh-cells and that with the infinite ground has 600,848 mesh-cells; their run times are 684 s and 577 s, respectively.

The final design is $\boldsymbol{x}^* = [5.9\ 1.05\ 7.825\ 5.9\ 1.8\ 7.95\ 4.75\ 0.90\ 7.75\ 13.50\ 10.0\ 18.40]^T$. Figure 7 shows the reflection responses of the DRA at the optimized design. The far field responses of the final design at selected frequencies are shown in Fig. 8.

The total design cost corresponds to about 20 high-fidelity model evaluations, which shows that our optimization procedure is quite efficient taking into account the number of design variables. It follows from the responses shown in Fig. 7(b) that it would be possible to obtain better designs for the DRA for each installation case considered separately. Our final design is a compromise ensuring that the DRA satisfies the design specifications for both considered scenarios.

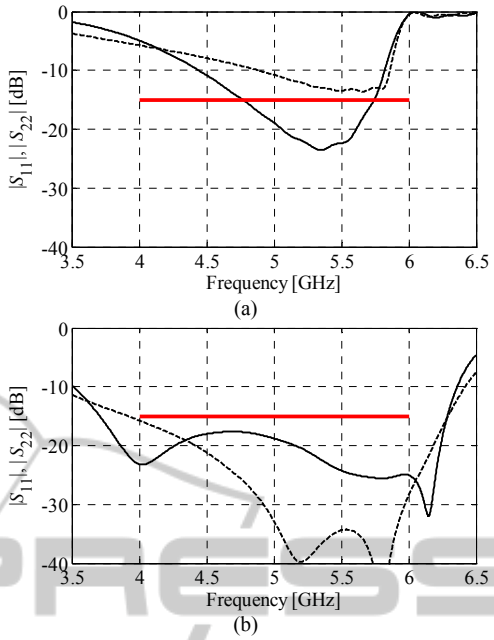

Figure 7: $|S_{11}|$ of the initial, (a), and optimized, (b), designs: at the finite (—) and infinite (– –) ground. Specifications are shown with the thick solid line.

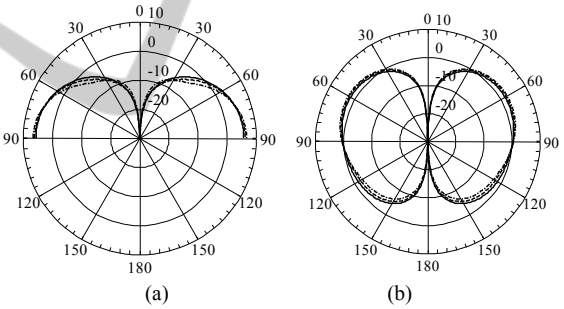

Figure 8: Gain [dBi] of the final design in the elevation plane (a) DRA at the infinite ground, and (b) DRA with the finite ground at 4.5 GHz (—), 5.0 GHz (– –), and 5.5 GHz (– · – ·).

3.3 Dual Rectangular DRA with a Substrate Integrated Cavity using Kriging and SM

Consider a DRA shown in Fig. 9 and 10. It has two mutually coupled rectangular DRs (Deng et al., 2004) which are installed at a printed circuit board (PCB) layer. The layer has the upper and lower metal grounds, and its dielectric substrate is 2.5 mm thick RT6010. The relative permittivity and loss tangent of the DRs are 36 and 10^{-4}. The DRs are in polycarbonate housing (relative permittivity of 2.7 and dielectric loss tangent of 0.01). The housing is fixed to the board with four bolts. Feeding of the

DRA is with a 50 ohm grounded coplanar waveguide (GCPW). The GCPW is terminated by two symmetrical slots (width s_1 and length x_1, see Fig. 10(a)). Figures 9 and 10(a) also show vias forming a substrate integrated cavity. The $TE^{x}_{\delta 11}$ mode is excited in the DRA.

Dimensions of the DRA are to be adjusted for the following design requirements: input reflection coefficient, $|S_{11}|$, should be better than –20 dB, and gain is to be higher than 3dBi for $\theta = 0^0$ (Z-direction), both over the 2.4-to-2.5 GHz band.

There are eleven design variables: $\boldsymbol{x} = [x_0\ y_0\ x_d\ y_d\ z_d\ s_1\ x_1\ x_v\ y_v\ s_x\ s_y]^T$, where x_0 and y_0 are location of the center of one DR relative to the origin of the coordinate system marked by O in Fig. 10; x_d, y_d, and z_d are dimensions of the DRs (ceramic body); s_1 and x_1 are dimensions of the slots energizing the DRs; x_v, y_v, s_x, and s_y describe via locations and in row spacing as shown in Fig. 10(a). The substrate integrated cavity is defined with ten vias in the lower (horizontal) row, eleven vias in the upper (horizontal) row, and nine vias in the vertical rows, see Fig. 10(a). Other dimensions are fixed as follows. Dimensions of the GCPW are signal trace width, w_0, of 1.5 mm and spacing, s_0, of 1mm. Diameter of the vias, d_v, is 1.5 mm.

Thicknesses of the polycarbonate housing, x_h, y_h, and z_h, are 2 mm. Location of the mounting bolts are described by $x_h = s_x$ and $y_h = 1$ mm. The heads of the bolts are 4 mm in diameters and 1 mm tick. Lateral extension of the housing is $l_h = x_v + 5s_x + 3$ [mm]. The whole structure has a magnetic symmetry plane which is shown with vertical dash-dot lines in Fig. 10. Ground plane and GCPW signal trace metallization is with 1.5 oz (0.05 mm thick) copper.

Design starts from $\boldsymbol{x}^{init} = [x_0\ y_0\ x_d\ y_d\ z_d\ s_1\ x_1\ x_v\ y_v\ s_x\ s_y]^T = [7.75\ 5\ 6\ 16.5\ 18\ 2\ 10.75\ 6\ 14\ 4\ 6]^T$ mm. The final design was found to be $\boldsymbol{x}^* = [7.62\ 5.70\ 6.2\ 16.43\ 17.9\ 1.9\ 10.45\ 6.08\ 13.83\ 4.37\ 6.03]^T$ mm. The design response meets the specifications; its $|S_{11}|$ is shown in Fig. 11, the gain versus frequency for $\theta = 0^0$ is shown in Fig. 12, and the gain pattern cuts at 2.45 GHz are shown in Fig. 13.

For the purpose of comparison, the DRA without substrate integrated cavity was also considered. In this case there were seven design variables $\boldsymbol{x}^{*n.v.} = [x_0\ y_0\ x_d\ y_d\ z_d\ s_1\ x_1]^T$. Figures 14 and 15 give responses of the two alternative designs, $\boldsymbol{x}^{*n.v}$ = $[7.65\ 5.51\ 5.39\ 16.20\ 19.45\ 0.263\ 10.05]^T$ mm ($|S_{11}| < -11.5$ dB, gain ($\theta = 0^0$) > 2.5dBi) and $\boldsymbol{x}^{**n.v}$ = $[6.79\ 5.25\ 5.68\ 16.22\ 19.97\ 0.250\ 9.46]^T$ mm ($|S_{11}| < -13.5$ dB, gain ($\theta = 0^0$) > 0.5dBi). The difference in the gains (Figs. 14 and 15) is due to the parasitic signal emission into substrate happening in the via-less designs.

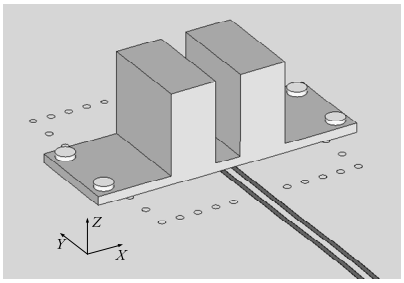

Figure 9: DRA, 3D view: two rectangular DRs in a housing; feeding is with a GCPW.

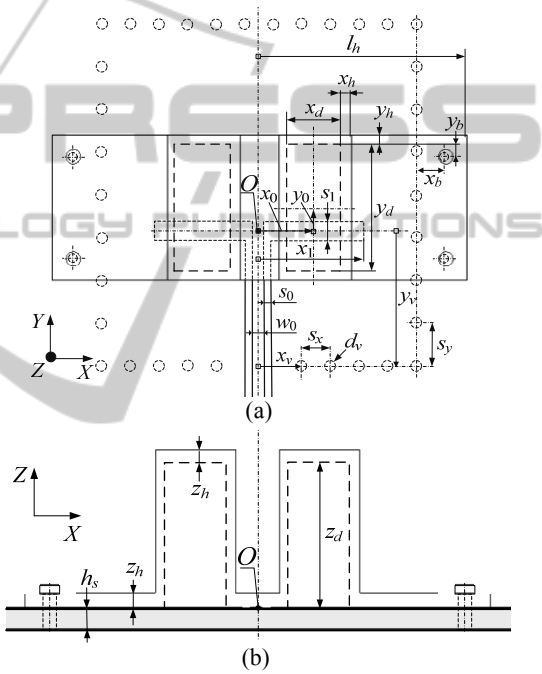

Figure 10: DRA layout: (a) top view; (b) front view (vias forming substrate integrated cavity not shown).

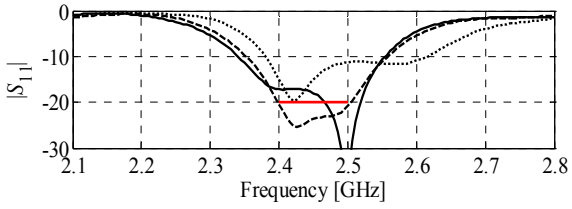

Figure 11: Simulation-driven design procedure (first stage): $|S_{11}|$ response of the coarse-discretization DRA model at the initial design (· · ·), $|S_{11}|$ of the coarse-discretization model at its optimized design (- - -), and $|S_{11}|$ of the high-fidelity model at the coarse-discretization model optimum (—). Specifications are shown with the horizontal line.

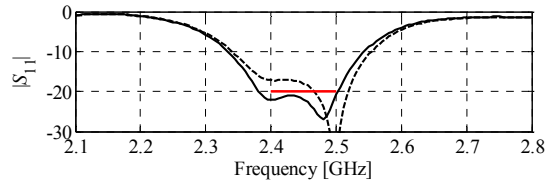

Figure 12: Simulation-driven design procedure (second stage): $|S_{11}|$ response of the high-fidelity model at the coarse-discretization model optimum (- - -), and at the final design obtained using space-mapping optimization with kriging coarse model (—).

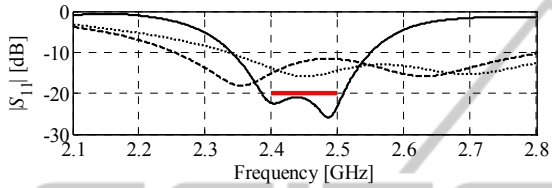

Figure 13: DRA, $|S_{11}|$ response at the final design: with substrate integrated cavity, $\boldsymbol{x}^*$ (—); no vias, $\boldsymbol{x}^{*n.v}$ (- - -); and no vias, $\boldsymbol{x}^{**n.v.}$ (· · ·).

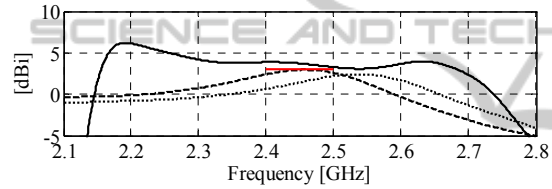

Figure 14: DRA, gain response in *Z*-direction at the final design: with substrate integrated cavity, $\boldsymbol{x}^*$ (—); no vias, $\boldsymbol{x}^{*n.v}$ (- - -); and no vias, $\boldsymbol{x}^{**n.v.}$ (· · ·). Design specifications shown with the horizontal line.

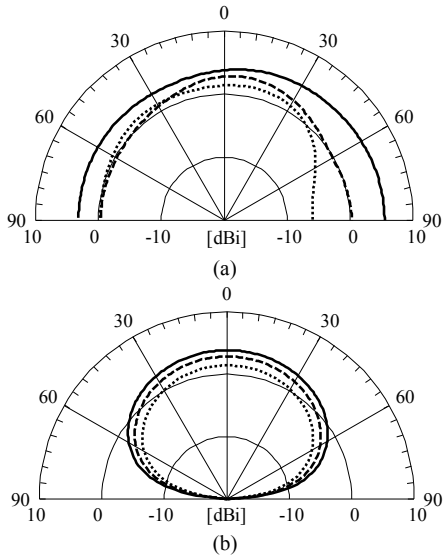

Figure 15: DRA, gain at 2.45 GHz (a) co-pol. in the *E*-plane (*YOZ*), the right sector is for the positive *Y*-direction; (b) x-pol. in the *H*-plane (*XOZ*). Design with substrate integrated cavity, $\boldsymbol{x}^*$, (—); designs without vias, $\boldsymbol{x}^{*n.v}$ (- - -) and $\boldsymbol{x}^{**n.v.}$ (· · ·).

3.4 Discussion

All the methods considered in this paper have been demonstrated (Section 3) to yield an optimized DRA design at the computational cost corresponding to a few high-fidelity EM simulations of the antenna structure of interest.

The first two methods, SPRP and AADS are simple to implement, however, they both require the responses of the low- and high-fidelity model (here, $|S_{11}|$ versus frequency) to be similar in shape. SPRP is a response correction technique and it requires that the distinctive features of responses for both models correspond to each other (Koziel, 2010b). AADS is not that restrictive with respect to the relationship between the model responses, however, it is most suitable for simple design specifications (e.g., single requirement for $|S_{11}|$, see Section 3.2). With SPRP, on the other hand, it is more straightforward to handle multiple objectives and constraints.

The last method, space mapping with kriging-based coarse models (Section 2.3) is more general than SPRP and AADS in the sense that it can handle the cases when the low- and high-fidelity model responses are more misaligned. However, SM is more difficult to implement and requires more experience from the user in order to set it up properly (Koziel et al., 2008).

4 CONCLUSIONS

Computationally efficient simulation-driven design of dielectric resonator antennas is discussed. The techniques described here exploit low-fidelity DRA models obtained through coarse-discretization EM simulations as well as various correction methods that aim at constructing a reliable surrogate model of the DRA structure under consideration. We demonstrate that the optimized designs can be obtained at a low computational cost corresponding to a few high-fidelity full-wave electromagnetic simulations of the DRA of interest.

ACKNOWLEDGEMENTS

The authors thank CST AG, Darmstadt, Germany, for making CST Microwave Studio available. This work was supported in part by the Icelandic Centre for Research (RANNIS) Grant 110034021.

REFERENCES

Amari, S., LeDrew, C., and Menzel, W., 2006, Space-Mapping Optimization of Planar Coupled-Resonator Microwave Filters. *IEEE Trans. Microwave Theory Tech.*, 54(5), pp. 2153-2159.

Bandler, J. W., Cheng, Q. S., Dakroury, S. A., Mohamed, A.S., Bakr, M.H., Madsen, K., and Søndergaard, J., 2004, Space Mapping: The State of The Art. *IEEE Trans. Microwave Theory Tech.*, 52(1), pp. 337-361.

CST Microwave Studio, ver. 2010, CST AG, Bad Nauheimer Str. 19, D-64289 Darmstadt, Germany, 2010.

Deng, S. M., Tsai, C. L., Chiu, C. W., Chang, S. F., 2004, CPW-fed dual rectangular ceramic dielectric resonator antennas through inductively coupled slots. *IEEE Antennas Propag. Soc. Int Symp.*, 1, pp. 1102-1105.

Deslandes, D., and Wu, K., 2005, Analysis and Design of Current Probe Transition from Grounded Coplanar to Substrate Integrated Rectangular Waveguides. *IEEE Trans. Microw. Theory Tech.*, 53, pp. 2487-2494.

De Young, C. S., Long, S. A., 2006, Wideband cylindrical and rectangular dielectric resonator antennas. *IEEE Antennas Propag. Lett.*, 5(1), pp. 426-429.

Forrester, A. I. J., Keane, A. J., 2009, Recent Advances in Surrogate-Based Optimization. *Prog. in Aerospace Sciences*, 45(1-3), pp. 50-79.

Guo, Y.-X., Ruan, Y.-F., Shi, X.-Q., 2005, Wide-band stacked double annular-ring dielectric resonator antenna at the end-fire mode operation, *IEEE Trans. Antennas Propag.,* 53(10), pp. 3394-3397.

Haupt, R. L., 2007, Antenna Design with A Mixed Integer Genetic Algorithm. *IEEE Trans. Antennas Propag.*, 55(3), pp. 577-582.

Kishk, A. A., Antar, Y. M. M., 2007, Dielectric Resonator Antennas, in *Antenna Engineering Handbook*, 4th ed., Volakis, J.L., Editor, McGraw-Hill.

Kolda, T.G., Lewis, R.M., Torczon, V., 2003, Optimization by direct search: new perspectives on some classical and modern methods. *SIAM Rev.*, 45(3), pp. 385–482.

Koziel, S., Bandler, J.W., and Madsen, K., 2006, A Space Mapping Framework for Engineering Optimization: Theory and Implementation. *IEEE Trans. Microwave Theory Tech*., 54(10), pp. 3721-3730.

Koziel, S., Cheng, Q.S., and Bandler, J.W., 2008, Space Mapping. *IEEE Microwave Magazine*, 9(6), pp. 105-122.

Koziel, S., Meng, J., Bandler, J. W., Bakr, M. H., and Cheng, Q.S., 2009a, Accelerated Microwave Design Optimization with Tuning Space Mapping. *IEEE Trans. Microwave Theory and Tech.*, 57(2), pp. 383-394.

Koziel, S., 2009b, Surrogate-based optimization of microwave structures using space mapping and kriging. *European Microwave Conference*, Rome, Italy, pp. 1062-1065.

Koziel, S., 2010a, Adaptively Adjusted Design Specifications for Efficient Optimization of Microwave Structures. *Progress in Electromagnetic Research B (PIER B)*, 21, pp. 219-234.

Koziel, S., 2010b, Shape-preserving response prediction for microwave design optimization. *IEEE Trans. Microwave Theory and Tech.*, 58(11), pp. 2829-2837.

Lizzi, L., Viani, F., Azaro, R., and Massa, A., 2007, Optimization of A Spline-Shaped UWB Antenna by PSO. *IEEE Antennas Wireless Propag. Lett.*, 6, pp. 182–185.

Petosa, A., 2007, *Dielectric Resonator Antenna Handbook*. Artech House.

Ong, S.W., Kishk, A. A., Glisson, A. D., 2002, Wideband disc-ring dielectric resonator antenna. *Microwave Optical Tech. Lett.*, 35(6), pp. 425-428.

Queipo, N. V., Haftka, R. T., Shyy, W., Goel, T., Vaidynathan, R., and Tucker, P.K., 2005, Surrogate-Based Analysis and Optimization. *Progress in Aerospace Sciences*, 41(1), pp. 1-28.

Rautio, J.C., 2007, EM-Component-Based Design of Planar Circuits. *IEEE Microwave Magazine*. 8(4), pp. 79-90.

Rocca, P., Manica, L., Stringari, F., Massa, A., 2008, Ant Colony Optimization for Tree-Searching-Based Synthesis of Monopulse Array Antenna. *Electronic Letters*, 44(13), pp. 783 – 785.

Shum, S., Luk, K., 1995, Stacked anunular ring dielectric resonator antenna excited by axi-symmetric coaxial probe, IEEE Trans. Microwave Theory Tech., 43(8), pp. 889-892.

Yang, X.-S., 2010, *Engineering Optimization: An Introduction with Metaheuristic Applications*, Wiley.